BEILSTEIN JOURNAL OF NANOTECHNOLOGY

Nonmonotonous temperature dependence of Shapiro steps in YBCO grain boundary junctions

Leonid S. Revin*[1,2], Dmitriy V. Masterov[1], Alexey E. Parafin[1], Sergey A. Pavlov[1] and Andrey L. Pankratov[1,2,3]

Full Research Paper

Open Access

Address:
[1]Institute for Physics of Microstructures of RAS, GSP-105, Nizhny Novgorod, 603950, Russia, [2]Center of Quantum Technologies, Nizhny Novgorod State Technical University, Nizhny Novgorod, Russia and [3]Lobachevsky State University of Nizhny Novgorod, Nizhny Novgorod, Russia

Email:
Leonid S. Revin* - rls@ipmras.ru

* Corresponding author

Keywords:
characteristic frequency; Shapiro steps; temperature dependence; YBaCuO Josephson junction

Beilstein J. Nanotechnol. **2021,** *12,* 1279–1285.
https://doi.org/10.3762/bjnano.12.95

Received: 08 September 2021
Accepted: 02 November 2021
Published: 23 November 2021

This article is part of the thematic issue "Intrinsic Josephson effect and prospects of superconducting spintronics".

Guest Editor: A. S. Sidorenko

Abstract

The amplitudes of the first Shapiro steps for an external signal with frequencies of 72 and 265 GHz are measured as function of the temperature from 20 to 80 K for a 6 μm Josephson grain boundary junction fabricated by YBaCuO film deposition on an yttria-stabilized zirconia bicrystal substrate. Non-monotonic dependences of step heights for different external signal frequencies were found in the limit of a weak driving signal, with the maxima occurring at different points as function of the temperature. The step heights are in agreement with the calculations based on the resistively–capacitively shunted junction model and Bessel theory. The emergence of the receiving optima is explained by the mutual influence of the varying critical current and the characteristic frequency.

Introduction

High-temperature superconducting (HTSC) Josephson junctions (JJs) are of great interest since many physical properties can be observed in dynamics during the changing the temperature within a wide range from nitrogen temperatures down to sub-kelvin, such as the phase diffusion regime [1-3], evidence for a minigap [4], and low-noise nano-junctions [5]. Such abilities raise not only fundamental interest in HTSC JJs but also an active search for ways to practically use such JJs. In recent years, the limiting characteristics of detectors and mixers based on HTSC JJs [6-11] have been actively studied. Josephson junctions have also been used for various spectroscopic applications [12]. In this area, the AC Josephson effect is utilized for the Hilbert-transform spectral analysis [13,14].

It should be noted that the simplest marker of the response level of a Josephson junction to microwave (MW) radiation is the

magnitude of Shapiro steps. In the majority of works, an increase in sensitivity at low temperatures has been demonstrated [15-17], although a part of the papers indicate the receiver's operation optimum at intermediate temperatures between the liquid nitrogen and helium temperatures [18,19]. The issue of obtaining sharp Shapiro steps is especially important for the development of HTSC Josephson voltage standards, consisting of series arrays of up to tens of thousands Josephson junctions [20,21]. Biased at frequencies in the range of $\omega/(2\pi)$ = 70–90 GHz, such arrays provide accurate quantized voltages $V_n = n\hbar\omega/(2e)$ exceeding 10 V. This accuracy is particularly determined by the magnitude of the response to external radiation. The Shapiro step observation can also be used as a clear probe to the gap symmetry of multigap superconductors [22].

The heights of the MW-induced voltage steps have been measured as a function of the MW power for various Josephson weak links fabricated from high-T_c superconductors [16,23,24]. The measured amplitudes are often smaller than those predicted by the resistively–capacitively shunted-junction (RCSJ) model [25,26], especially for measurements obtained at high temperatures. However, taking into account the effect of the YBCO junction resistance thermal noise [16] makes it possible to neutralize this difference and obtain a good agreement between the experiment and the theory.

While for low-temperature JJs the temperature dependence of the Shapiro steps is weak [27], for HTSC junctions the response to a MW signal has a general tendency to rise with decreasing temperature, but may have peculiarities for certain sample parameters [19].

In this paper, we investigate the temperature dependence of the first Shapiro step amplitude for an external signal with frequencies of 72 and 265 GHz acting on $YBa_2Cu_3O_{7-\delta}$ 6 μm Josephson grain boundary junction. The observed non-monotonous behavior of the step height in the limit of low signal power is discussed, and the measurement results are compared with the results of numerical calculations.

Experimental Setup and Numerical Model

The samples of grain boundary Josephson junctions were fabricated by on-axis dc magnetron sputtering [28-31] of $YBa_2Cu_3O_{7-\delta}$ (YBCO) film on the surface of 24°[001]-tilt $Zr_{1-x}Y_xO_2$ bicrystal substrates with modification of the substrate surface by preliminary topology masks [29,30]. The junctions with length L = 6 μm along the grain boundary and thickness 0.3 μm were integrated into a dipole antenna. The structure look follows the design from [29]. Based on the analysis of the transport properties, the best structure was selected and located at the center of a Si lens for efficient detection. The sample was mounted into a dry cryostat allowing for measurements in a wide temperature range from helium temperatures to ≈80 K. An external gigahertz signal was fed through an optical window with IR filters using a semiconductor synthesizer with a multiplier (70–78 GHz) or using a backward wave oscillator (230–370 GHz). The JJ transport properties and the response were characterized by a precise Keithley low-noise current source and nanovoltmeter using a standard 4-probe technique.

In the RCSJ model to which we compare our experimental results, the junction phase ϕ with an ideal critical current I_c, a resistance R_N and a capacitance C are described by the stochastic differential equation [32,33]

$$I = I_c \sin\phi + \frac{V}{R_N} + C\frac{dV}{dt} + I_{mw}\sin\left(2\pi F_{mw}t\right) + I_F, \quad (1)$$

where the voltage $V = d\phi/dt \times 2\pi/\Phi_0$ (Φ_0 is the magnetic flux quantum). The thermal fluctuations I_F are assumed to be a white Gaussian noise with zero mean and correlation function

$$\left\langle I_F(t) I_F(t+\tau)\right\rangle = \frac{k_B T}{\pi R_N}\delta(\tau).$$

A simple harmonic signal of the amplitude I_{mw} and the frequency $\omega_{mw} = 2\pi F_{mw}$ describes an external high-frequency radiation of the power $P_{mw} = I_{mw}^2 R_N/2$. Its effect on the Josephson system particularly depends on the characteristic frequency $\omega_c = 2eI_cR_N/\hbar$ of the JJ.

Results

First, the current–voltage characteristics (IVCs) were measured, and the value of the critical current as a function of temperature was found, see Figure 1. The $I_c(T)$ dependence is similar to the experimental observations for other such structures [34-36]. At the same time, the normal resistance of the JJ remained virtually constant, that is, R_N was 0.23–0.24 Ω within the whole studied temperature range. For the subsequent analysis of the results, we used data from the literature about similar structures of an YBCO bicrystal junction on 24°[001]-tilt $Zr_{1-x}Y_xO_2$ substrate [37] as the value of the junction capacitance $C = 3 \times 10^{-2}$ F/m^2 × 1.8 × 10^{-12} m^2 = 0.05 pF. This value, according to [35], remains almost unchanged over a wide temperature range.

It is important to understand which parameters vary in the model with the temperature. Figure 1 also shows the change in the Josephson junction characteristic length L/λ_J, where $\lambda_J = \sqrt{\Phi_0/(2\pi\mu_0 J_c d)}$ is the Josephson penetration depth,

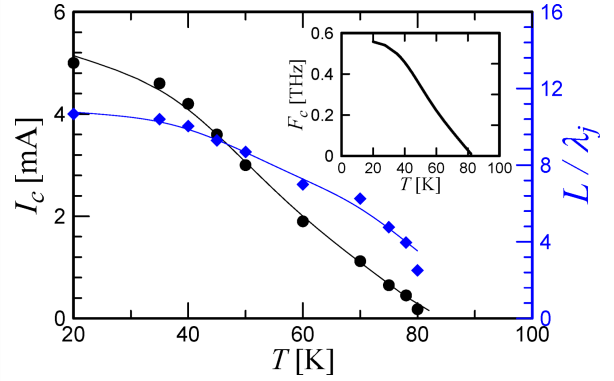

Figure 1: The dependence of the critical current (black dots) and the characteristic length of the Josephson junction (blue diamonds) on the temperature. The solid curves are spline approximations. The inset shows $F_c = \omega_c/(2\pi)$ versus T.

which determines the size of a fluxon in the junction. Here μ_0 is the vacuum permeability, J_c is the critical current density, and $d = t + 2\lambda_L$ is the effective magnetic thickness with the junction barrier thickness t = 1.5 nm and the London penetration depth λ_L = 250–150 nm [38]. It can be seen from the figure that, for nitrogen temperatures, the Josephson junction can generally be considered as a short JJ. With the decrease in the temperature, its characteristic dimension increases, and for 20 K, in the general case, Equation 1 becomes invalid, that is, the dynamics of the spatial distribution of the phase and the magnetic field inside the junction becomes important [39-41]. In the case of long JJs it is necessary to consider the sine-Gordon equation, taking into account the non-uniform distribution of currents flowing through the barrier, which is typical for bicrystal junctions [28,42,43]. However, if the junction length is of the order of the kink size and there is no external magnetic field, the long junction dynamics is close to that of a short one [39] and the used model is qualitatively adequate. This is confirmed in [40], where the escape time from the superconducting state is investigated, and it is shown that the critical length L/λ_J = 5 corresponds to the crossover between two dynamical regimes. Nevertheless, long HTSC junctions are characterized by such features as a flux creep and the change in the IVC curvature associated with the crossover from the flux flow to Josephson junction behavior [44]. That is why, as it will be shown below, in the region of low temperatures, the agreement between the experiment and the numerical calculation is not as good as in the region of high T values.

The second important parameter is the characteristic frequency ω_c (or F_c) (see the inset of Figure 1). The change of ω_c radically affects the response of the system to an external MW signal [17]. Essentially, the ω_{mw}/ω_c (or F_{mw}/F_c) ratio determines if the detection regime is optimal for the junction. This issue is discussed in more details below.

The third important parameter is the thermal noise magnitude, k_BT, which affects the smearing of the Shapiro steps, and, accordingly, the decrease in the step size in the region of low radiation power. It is not shown in Figure 1.

Figure 2 shows the IVCs for temperatures of 70 and 50 K in the absence of a high-frequency signal and in the regime of detecting external 72 or 265 GHz signals. The measurement results are in good agreement with the numerical simulations (the black curves). It should be noted that the radiation power was the same for the measurements at all temperatures. The power level of the two signals, 72 and 265 GHz, was chosen to be near the first minimum of the critical current, and, accordingly, near the first maximum of the first Shapiro step at high temperatures. This can be seen from the IVC for T = 70 K and F_{mw} = 72 GHz: the critical current is nearly zero, the amplitude of the first step is greater than the amplitude of the second and the third steps. The same picture is observed for the IVC at F_{mw} = 265 GHz. The comparison with the numerical model gives an estimate of the power absorbed by the Josephson junction: it is 0.4 μW for 72 GHz, and P_{mw} = 3 μW for 265 GHz.

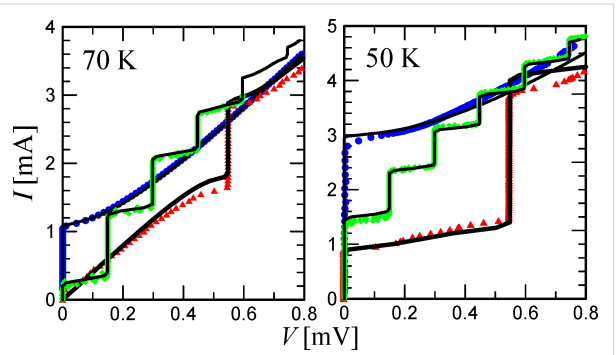

Figure 2: IVCs of a Josephson junction without an MW signal (blue dots), under the action of an external signal of 72 GHz (green diamonds) and 265 GHz (red triangles) at temperatures of 70 and 50 K. The black lines are the numerical calculations for each curve with the experimental parameters and with fitting power P_{mw}.

Figure 3, essentially the main result of the article, demonstrates the dependence of the first Shapiro step amplitude on the temperature for 72 and 265 GHz radiation at a constant power. The dependences are non-monotonic and have a maximum located at different temperature values for different MW frequencies. In addition, it can be seen that at high temperatures of approx. 80 K, the amplitudes of the steps are close, while with decreasing temperature in the case of 265 GHz radiation, the Shapiro steps become significantly higher than for 72 GHz. The numerical results (the solid curves) based on the experimental data

describe the experiment at high temperatures well and differ quantitatively at low temperatures. This may be caused by a specific dynamics arising with an increase in the characteristic length of the JJ at low temperatures. Nevertheless, the simulation qualitatively follows the experimental dependence within the entire temperature range.

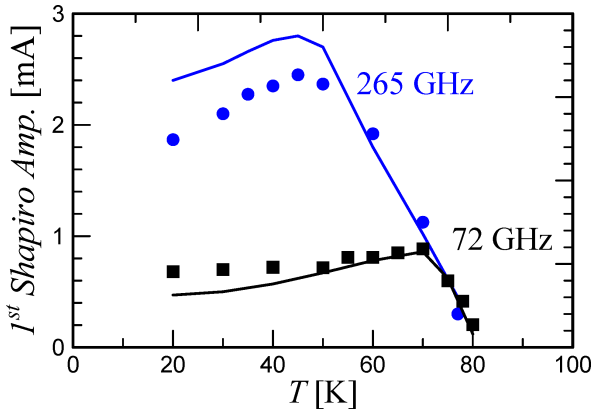

Figure 3: The dependence of the first Shapiro step amplitude on the temperature for 72 and 265 GHz radiation at a constant power. The dots are the experimental values, the lines are the theory for the temperatures at which the measurements were conducted.

The obtained effect of the optimum in the JJ response is associated with a simultaneous change of several parameters when the temperature changes. For a qualitative analysis, let us consider the expression for the first Shapiro step amplitude [33,45,46]:

$$\Delta I_1 = I_c \sum_{k=-\infty}^{+\infty} J_k(a) J_{-1-k}(a) \left| I_p\left[\left(k-\frac{1}{2}\right)\omega_{mw}\right]\right|, \quad (2)$$

where J_k and J_{-1-k} are Bessel functions at $a = \frac{I_{mw}}{2I_c\omega_{mw}/\omega_c}$, I_p is a complex function that determines the quadrature components of the supercurrent depending on the Josephson generation frequency. Although this expression is valid for a voltage-biased JJ, it is in a good agreement with measurements for the current-biased regime and RCSJ model [35]. In the case of low signal power and $\omega_{mw} \ll \omega_c$, the maximum height of the first step is proportional to

$$\max \Delta I_1 \approx I_c\omega_{mw}/\omega_c\,. \quad (3)$$

In the limit of $\omega_{mw} \approx \omega_c$, the expression for ΔI_1 takes the simple form:

$$\Delta I_1 \approx 2I_c \left| J_1\left(\frac{I_{mw}}{2I_c\omega_{mw}/\omega_c}\right)\right|. \quad (4)$$

Figure 4 shows the theoretical dependence of $\max\Delta I_1$ on the frequency for various temperatures. According to Equation 3, the maximum step amplitude increases as the critical current increases and the temperature goes down. At the same time, due to the change in the critical frequency ω_c (the inset in Figure 1), the optimal signal detection regime is shifted. That is, for temperatures of 80 K and 70 K and the frequency of 72 GHz, the condition $\omega_{mw} \approx \omega_c$ is satisfied, and the step heights reach $\approx I_c$ and $\approx 0.9\ I_c$, respectively. At 50 K, $\max\Delta I_1 \approx I_c\omega_{mw}/\omega_c = I_cF_{mw}/F_c = 3$ mA × 72 GHz/330 GHz = 0.65 mA, and at 20 K, $\max\Delta I_1 \approx 5$ mA × 72 GHz/560 GHz = 0.64 mA. For 265 GHz signal, the step height almost reaches the limit $\approx I_c$ at 50 K, while at 20 K, ω_{mw} is still far from ω_c. Summarizing, for low-gigahertz radiation frequencies, lowering the temperature does not gain the response magnitude due to the non-optimal frequency of signal detection. Whereas, the closer ω_{mw} to the characteristic frequency, the greater the influence of the critical current increase with the temperature takes place.

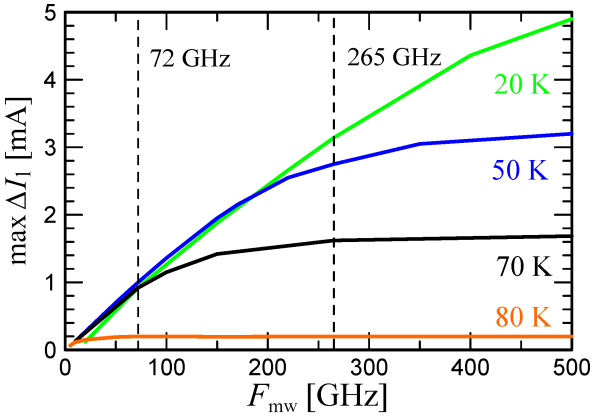

Figure 4: max ΔI_1 as function of F_{mw} at various temperatures. The dotted lines mark the position of the two frequencies used in the experiment.

In addition to the magnitude of the Shapiro step height maximum, it is important to take into account the period of the Bessel function, which, in the first approximation, determines the response of the JJ to a change in the gigahertz-signal power. Equation 4 shows that as ω_c grows, the Bessel function period increases, that is, the derivative $d\Delta I_1/dP_{mw}$ decreases. Figure 5 shows the results of the numerical calculations of the first Shapiro step height versus the external signal power at the temperatures of 70, 50, and 20 K. The upper panel of Figure 5 corresponds to the external signal frequency of 72 GHz. It can be seen that $\max\Delta I_1$ is close for all three temperatures, as explained earlier, see Figure 4. Nonetheless, due to the shift in the step maximum position in power, for small signal levels (marked with a vertical dashed line), ΔI_1 at 70 K is larger than at 50 and 20 K. The bottom panel of Figure 5 corresponds to a

265 GHz external signal. Here, for different temperatures, there is also a shift in the position of the Shapiro step maximum along the power axis, but it is smaller in comparison with the previous case, since ω_{mw}/ω_c is closer to unity. In this case, the increase in the maximum step height with temperature is also significant. Nevertheless, there is an optimum ΔI_1 in temperature due to the competition between two effects, namely an increase in $\max\Delta I_1$ with an increase in the critical current and a decrease in $d\Delta I_1/dP_{mw}$ with an increase in the critical current.

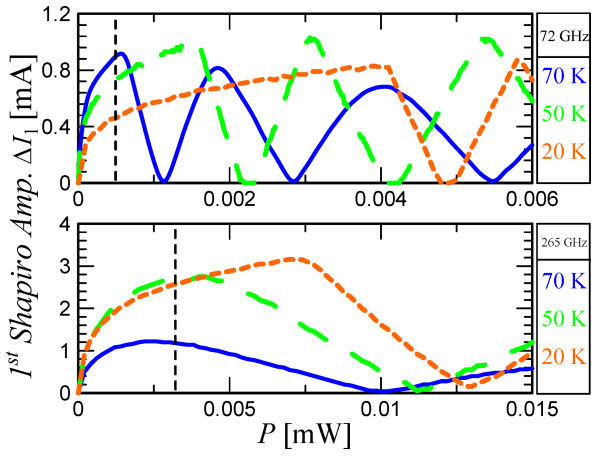

Figure 5: The first Shapiro step as function of P_{mw} at three temperatures and under a signal at 72 GHz (upper graph) and 265 GHz (lower graph). The black dashed lines indicate the power levels from the experiment.

Conclusion

The response in the form of the amplitudes of the Shapiro steps to an external signal with frequencies of 72 and 265 GHz was measured for 6 μm YBaCuO bicrystal junctions as a function of temperature in the range from 20 to 80 K. Nonmonotonic dependences of the step height were found in the region of a weak external signal with maxima at various points. The heights of the steps are consistent with calculations based on the RCSJ model and are qualitatively described by Bessel functions. The occurrence of the receiving optima is explained by the mutual influence of the varying critical current and the characteristic frequency. The maximum response to a 72 GHz signal has an optimum at 70 K, while to a 265 GHz signal – at 50 K.

For applied tasks of terahertz imaging [47], mixing [36], and Hilbert-transform spectral analysis [13] it is not possible to vary the incident power over a wide range. The power level is set there by losses, mismatch, and power absorption by the samples under study. Moreover, in applied problems one has to deal with low power levels and a linear response of detector [48]. Specifically in this area of the device operation, the effect described in the paper can be observed.

The obtained optima arise at certain JJ parameters (R_N, $I_c(T)$, C, and $\omega_c(T)$). Depending on these parameters, such maxima may appear [18,19] or not appear [17] in the measurements at an intermediate temperature. For specific purposes and operation regions, it is possible to tune JJ parameters to operate in the optimal regime [47,49]. In addition to JJ characteristics, the operating frequency or the frequency range is important. For low ω_{mw}, the change in the response of the Josephson junction will be small with the temperature [16] since at these frequencies the detection is not optimal. At the same time, at high temperatures, thermal noise will blur the step more than at low temperatures, and with increasing I_c the step height will increase. This also applies to high frequencies close or greater than the gap. Non-monotonous peculiarities in the response will occur at intermediate frequencies at, in fact, the most interesting range from a practical point of view. The same optima of the response can be achieved in the operation temperature range at a low power of the external signal with a higher normal resistance and critical current of the sample.

Therefore, lowering the temperature for the HTSC does not necessarily lead to an improvement in the detection properties of the Josephson junctions. An interesting question for further investigation is the search for an analytical expression for the optimal temperature of receiving an external signal of a given power and frequency for given JJ parameters.

Funding

The work is supported by the Russian Science Foundation (Project No. 20-79-10384).

ORCID® iDs

Leonid S. Revin - https://orcid.org/0000-0003-1645-4122
Andrey L. Pankratov - https://orcid.org/0000-0003-2661-2745

References

1. Longobardi, L.; Massarotti, D.; Stornaiuolo, D.; Galletti, L.; Rotoli, G.; Lombardi, F.; Tafuri, F. *Phys. Rev. Lett.* **2012,** *109,* 050601. doi:10.1103/physrevlett.109.050601
2. Revin, L. S.; Pankratov, A. L.; Gordeeva, A. V.; Yablokov, A. A.; Rakut, I. V.; Zbrozhek, V. O.; Kuzmin, L. S. *Beilstein J. Nanotechnol.* **2020,** *11,* 960–965. doi:10.3762/bjnano.11.80
3. Massarotti, D.; Longobardi, L.; Galletti, L.; Stornaiuolo, D.; Rotoli, G.; Tafuri, F. *Low Temp. Phys.* **2013,** *39,* 294–298. doi:10.1063/1.4795203
4. Lucignano, P.; Stornaiuolo, D.; Tafuri, F.; Altshuler, B. L.; Tagliacozzo, A. *Phys. Rev. Lett.* **2010,** *105,* 147001. doi:10.1103/physrevlett.105.147001
5. Couëdo, F.; Amari, P.; Feuillet-Palma, C.; Ulysse, C.; Srivastava, Y. K.; Singh, R.; Bergeal, N.; Lesueur, J. *Sci. Rep.* **2020,** *10,* 10256. doi:10.1038/s41598-020-66882-1
6. Yu, M.; Geng, H.; Hua, T.; An, D.; Xu, W.; Chen, Z. N.; Chen, J.; Wang, H.; Wu, P. *Supercond. Sci. Technol.* **2020,** *33,* 025001. doi:10.1088/1361-6668/ab5e13

7. Sharafiev, A.; Malnou, M.; Feuillet-Palma, C.; Ulysse, C.; Wolf, T.; Couëdo, F.; Febvre, P.; Lesueur, J.; Bergeal, N. *Supercond. Sci. Technol.* **2018,** *31,* 035003. doi:10.1088/1361-6668/aa9d48
8. Malnou, M.; Feuillet-Palma, C.; Ulysse, C.; Faini, G.; Febvre, P.; Sirena, M.; Olanier, L.; Lesueur, J.; Bergeal, N. *J. Appl. Phys.* **2014,** *116,* 074505. doi:10.1063/1.4892940
9. Gao, X.; Du, J.; Zhang, T.; Jay Guo, Y.; Foley, C. P. *J. Infrared, Millimeter, Terahertz Waves* **2017,** *38,* 1357–1367. doi:10.1007/s10762-017-0422-x
10. Gao, X.; Zhang, T.; Du, J.; Weily, A. R.; Guo, Y. J.; Foley, C. P. *Supercond. Sci. Technol.* **2017,** *30,* 095011. doi:10.1088/1361-6668/aa7cc1
11. Yu, M.; Geng, H.; Jiang, S.; Hua, T.; An, D.; Xu, W.; Chen, Z. N.; Li, J.; Wang, H.; Chen, J.; Wu, P. *Opt. Express* **2020,** *28,* 14271. doi:10.1364/oe.390997
12. Chantry, G. W. *Submillimetre Spectroscopy;* Academic Press: London and New York, 1971.
13. Snezhko, A. V.; Gundareva, I. I.; Lyatti, M. V.; Volkov, O. Y.; Pavlovskiy, V. V.; Poppe, U.; Divin, Y. Y. *Supercond. Sci. Technol.* **2017,** *30,* 044001. doi:10.1088/1361-6668/aa5ab5
14. Divin, Y.; Poppe, U.; Gubankov, V. N.; Urban, K. *IEEE Sens. J.* **2008,** *8,* 750–757. doi:10.1109/jsen.2008.923185
15. Du, J.; Smart, K.; Li, L.; Leslie, K. E.; Hanham, S. M.; Wang, D. H. C.; Foley, C. P.; Ji, F.; Li, X. D.; Zeng, D. Z. *Supercond. Sci. Technol.* **2015,** *28,* 084001. doi:10.1088/0953-2048/28/8/084001
16. Kautz, R. L.; Ono, R. H.; Reintsema, C. D. *Appl. Phys. Lett.* **1992,** *61,* 342–344. doi:10.1063/1.107931
17. Pavlovskiy, V. V.; Divin, Y. Y. *J. Commun. Technol. Electron.* **2019,** *64,* 1003–1010. doi:10.1134/s106422691908014x
18. Lyatti, M. V.; Tkachev, D. A.; Divin, Y. Y. *Tech. Phys. Lett.* **2006,** *32,* 860–863. doi:10.1134/s1063785006100130
19. Konopka, J.; Wolff, I.; Beuven, S.; Siegel, M. *IEEE Trans. Appl. Supercond.* **1995,** *5,* 2443–2446. doi:10.1109/77.403085
20. Klushin, A. M.; Prusseit, W.; Sodtke, E.; Borovitskii, S. I.; Amatuni, L. E.; Kohlstedt, H. *Appl. Phys. Lett.* **1996,** *69,* 1634–1636. doi:10.1063/1.117055
21. Sosso, A.; Andreone, D.; Lacquaniti, V.; Klushin, A. M.; He, M.; Klein, N. *IEEE Trans. Appl. Supercond.* **2007,** *17,* 874–877. doi:10.1109/tasc.2007.898581
22. Ota, Y.; Machida, M.; Koyama, T. *Phys. Rev. B* **2010,** *82,* 140509. doi:10.1103/physrevb.82.140509
23. Gao, J.; Boguslavskij, Y.; Klopman, B. B. G.; Terpstra, D.; Gerritsma, G. J.; Rogalla, H. *Appl. Phys. Lett.* **1991,** *59,* 2754–2756. doi:10.1063/1.105878
24. Siegel, M.; Heinz, E.; Seidel, P.; Hilarius, V. *Z. Phys. B: Condens. Matter* **1991,** *83,* 323–326. doi:10.1007/bf01313400
25. Russer, P. *J. Appl. Phys.* **1972,** *43,* 2008–2010. doi:10.1063/1.1661440
26. Likharev, K. K.; Semenov, V. K. *Radio Eng. Electron Phys.* **1971,** *16,* 1917–1922.
27. Baars, P.; Richter, A.; Merkt, U. *Phys. Rev. B* **2003,** *67,* 224501. doi:10.1103/physrevb.67.224501
28. Revin, L. S.; Chiginev, A. V.; Pankratov, A. L.; Masterov, D. V.; Parafin, A. E.; Luchinin, G. A.; Matrozova, E. A.; Kuzmin, L. S. *J. Appl. Phys.* **2013,** *114,* 243903. doi:10.1063/1.4856915
29. Masterov, D. V.; Parafin, A. E.; Revin, L. S.; Chiginev, A. V.; Skorokhodov, E. V.; Yunin, P. A.; Pankratov, A. L. *Supercond. Sci. Technol.* **2017,** *30,* 025007. doi:10.1088/1361-6668/30/2/025007
30. Revin, L. S.; Pankratov, A. L.; Masterov, D. V.; Parafin, A. E.; Pavlov, S. A.; Chiginev, A. V.; Skorokhodov, E. V. *IEEE Trans. Appl. Supercond.* **2018,** *28,* 1100505. doi:10.1109/tasc.2018.2844354
31. Revin, L.; Pankratov, A.; Gordeeva, A.; Masterov, D.; Parafin, A.; Zbrozhek, V.; Kuzmin, L. *Appl. Sci.* **2020,** *10,* 7667. doi:10.3390/app10217667
32. Stephen, M. J. *Phys. Rev.* **1969,** *186,* 393–397. doi:10.1103/physrev.186.393
33. Likharev, K. K. *Dynamics of Josephson Junctions and Circuits;* Gordon and Breach Science Publishers: New York, 1986.
34. Il'ichev, E.; Zakosarenko, V.; IJsselsteijn, R. P. J.; Hoenig, H. E.; Meyer, H.-G.; Fistul, M. V.; Müller, P. *Phys. Rev. B* **1999,** *59,* 11502–11505. doi:10.1103/physrevb.59.11502
35. Rosenthal, P. A.; Grossman, E. N. *IEEE Trans. Microwave Theory Tech.* **1994,** *42,* 707–714. doi:10.1109/22.285085
36. Du, J.; Weily, A. R.; Gao, X.; Zhang, T.; Foley, C. P.; Guo, Y. J. *Supercond. Sci. Technol.* **2017,** *30,* 024002. doi:10.1088/0953-2048/30/2/024002
37. Zhang, Y. Dynamics and applications of long Josephson junctions. Ph.D. Thesis, Chalmers University of Technology, Göteborg, Sweden, 1993.
38. Il'ichev, E.; Dörrer, L.; Schmidl, F.; Zakosarenko, V.; Seidel, P.; Hildebrandt, G. *Appl. Phys. Lett.* **1996,** *68,* 708–710. doi:10.1063/1.116599
39. Fedorov, K. G.; Pankratov, A. L. *Phys. Rev. B* **2007,** *76,* 024504. doi:10.1103/physrevb.76.024504
40. Fedorov, K. G.; Pankratov, A. L. *Phys. Rev. Lett.* **2009,** *103,* 260601. doi:10.1103/physrevlett.103.260601
41. Gordeeva, A. V.; Pankratov, A. L. *Phys. Rev. B* **2010,** *81,* 212504. doi:10.1103/physrevb.81.212504
42. Revin, L. S.; Pankratov, A. L.; Chiginev, A. V.; Masterov, D. V.; Parafin, A. E.; Pavlov, S. A. *Supercond. Sci. Technol.* **2018,** *31,* 045002. doi:10.1088/1361-6668/aaacc3
43. Kupriyanov, M. Y.; Khapaev, M. M.; Divin, Y. Y.; Gubankov, V. N. *JETP Lett.* **2012,** *95,* 289–294. doi:10.1134/s0021364012060069
44. Hilgenkamp, H.; Mannhart, J. *Rev. Mod. Phys.* **2002,** *74,* 485–549. doi:10.1103/revmodphys.74.485
45. Kautz, R. L. *J. Appl. Phys.* **1995,** *78,* 5811–5819. doi:10.1063/1.359644
46. Braiman, Y.; Ben-Jacob, E.; Imry, Y. *IEEE Trans. Magn.* **1981,** *17,* 784–787. doi:10.1109/tmag.1981.1060952
47. Du, J.; Hellicar, A. D.; Hanham, S. M.; Li, L.; Macfarlane, J. C.; Leslie, K. E.; Foley, C. P. *J. Infrared, Millimeter, Terahertz Waves* **2011,** *32,* 681–690. doi:10.1007/s10762-010-9650-z
48. Lyatti, M.; Divin, Y.; Volkov, O.; Pavlovskii, V.; Gubankov, V.; Urban, K. *IEEE Trans. Appl. Supercond.* **2007,** *17,* 332–335. doi:10.1109/tasc.2007.898188
49. Gundareva, I.; Divin, Y. *IEEE Trans. Appl. Supercond.* **2016,** *26,* 1100204. doi:10.1109/tasc.2016.2520465